Far-field diffraction of linear chirped gratings

Luis Miguel Sanchez-Brea[a,*], Francisco Jose Torcal-Milla[b], Jeronimo Buencuerpo[a]

[a] *Optics Department, Applied Optics Complutense Group, Universidad Complutense de Madrid, Facultad de Ciencias Físicas, Plaza de las Ciencias 1, 28040, Madrid, (Spain).*
[b] *Applied Physics Department, Universidad de Zaragoza, 50009, Zaragoza (Spain).*

Abstract

We analyze the far-field diffraction pattern produced by linear spatial chirped gratings. An intuitive analytical interpretation of the generated diffraction orders is proposed for gratings with linear variation of the period and linear variation of the spatial frequency. Also, experiments using Gaussian beams and plane wave illumination are performed. The analytical expressions are compared to numerical and experimental results, showing a high agreement. Chirped gratings can be applied in interesting applications: we analyze how they can be used as a deflector, since tunable direction of diffracted orders can be achieved by displacing laterally the grating with respect to the incident light beam. Also the angular width of diffraction orders can be controlled and chirped gratings can be used to generate uniform illumination over a controlled angular range. These two applications have also been experimentally shown.

Keywords: chirped gratings, Diffraction, gratings

1. Introduction

Diffraction gratings are one of the most common optical elements, which consist of a periodical pattern that modulates the incident light beam. As it is well known, a diffraction grating produces diffraction orders at the far field that propagate along directions θ_n given by the grating equation, $p sin\theta_n = n\lambda$, where λ is the incident wavelength, n is an integer which represents the diffraction order, and p is the period of the grating, which typically is constant. In the recent years, quasi-periodic structures have aroused interest in the optical community [1, 2, 3, 4, 5, 6, 7, 8, 9, 10]. For example, in the temporal range, chirped fiber gratings are used as a solution for dispersion compensation [11]. In the spatial range, chirped gratings (CGs) have also been applied to produce curved diffraction orders [12], to extend the bandwidth in surface plasmon applications [13], as spectral selective elements in optical spectrometers and monochromators

*Corresponding author
Email address: optbrea@ucm.es (Luis Miguel Sanchez-Brea)

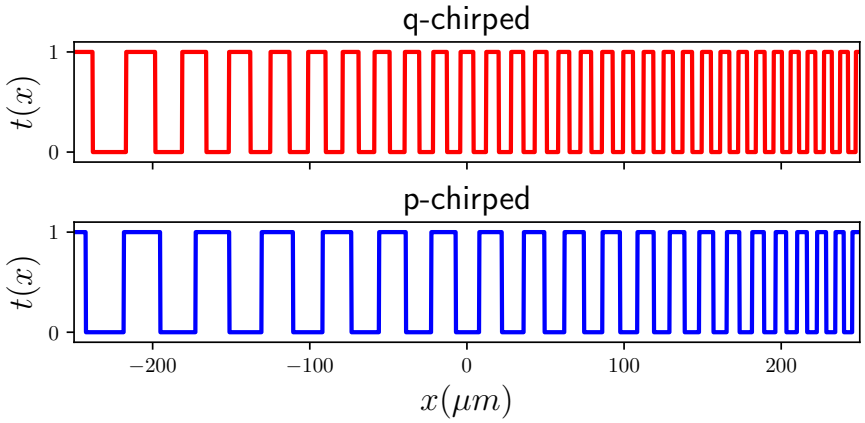

Figure 1: q- and p- chirped binary amplitude diffraction gratings with starting period $p_0 = 50\mu m$, final period $p_1 = 10\mu m$, and length $L = 500\mu m$.

[8, 14], in external cavity semiconductor laser diodes, [15, 16], and as a nanometer gap measurement device, [2]. Their advantages as focusing elements have been applied, [4], and they have also been used as reference marks in position optical encoders, [17].

From a theoretical point of view, CGs have been analyzed using a geometrical scheme [8], the ABCD matrix formalism [3], and also Fresnel approach for the near field (pseudo-self-imaging formation) [7]. Nevertheless, the far-field optical properties of CGs have not been investigated yet. Since CGs do not present a periodic structure, an analysis based on Fourier series and diffraction orders can only be performed in some particular cases. In this work, we analyze the far-field diffraction pattern produced by CGs of two kinds: p-chirped and q-chirped which correspond to linear variation of the period of the grating and linear variation of the spatial frequency of the grating respectively. Analytical expressions to explain the diffraction orders behavior produced by this kind of non-periodical grating are obtained, which are compared to numerical simulations and experimental results. Simulations based on Fast Fourier Transform and experimental results for q-chirped diffraction gratings are obtained, which corroborates the theoretical approach. Due to the structure of the far field diffraction pattern, CGs can be used in interesting applications, such as a deflector which can easily change the angle of the diffraction orders just moving the grating perpendicularly to the beam, or as a line generator since, for highly chirped gratings, the width of the diffraction orders can be controlled with the initial and final period of the grating.

2. Theoretical analysis

A CG of length L is defined in the real space by its initial and final periods, p_0 and p_1, and its variation rate of the lattice, p_a. Alternatively, in the reciprocal space the CG its defined by its initial and final spatial frequencies, $q_0 = 2\pi/p_0$ and $q_1 = 2\pi/p_1$ and its variation rate, q_a. We define two illustrative cases with linear variation in the real and reciprocal space, the p-chirped and q-chirped gratings

$$p(x) = p_c + p_a\, x, \qquad q(x) = q_c + q_a\, x, \tag{1}$$

where $p_c = (p_0+p_1)/2$, $p_a = (p_1-p_0)/L$, $q_c = (q_0+q_1)/2$, and $q_a = (q_1-q_0)/L$, respectively. The center of the grating is located, without loss of generality, at $x = 0$. Both gratings are generated by binarizing the sign of

$$t(x) = \text{bin}\left\{\cos\left[\int^x g(x')dx'\right]\right\}, \tag{2}$$

where $g(x')$ is replaced by the frequency for p- or q- CGs. Therefore, the q-CG is defined as

$$t_q(x) = bin\left[cos\left(\int^x q(x')dx'\right)\right] = bin\left[cos\left(q_c x + \frac{1}{2}q_a x^2\right)\right] \tag{3}$$

and the p-CG grating is defined as

$$t_p(x) = bin\left[cos\left(\int^x \frac{2\pi}{p(x')}dx'\right)\right] = bin\left[cos\left(\frac{2\pi}{p_a}log(p_c + p_a x)\right)\right]. \tag{4}$$

In Fig. 1 we can see an example of both gratings.

The next step is to analyze how these CGs behave in the far field when they are illuminated with a monochromatic Gaussian light beam whose beam width, ω_0, is placed at the plane of the CG, $z = 0$, and it is centered at x_g: $u_0(x) \propto exp[-(x - x_g)^2/\omega_0^2]$. Since the proposed p-CGs and q-CGs are not periodical, a simple analysis of the far field diffraction pattern is not possible. Nevertheless, after binarization, both p-chirped and q-chirped diffraction gratings can be described as

$$t_\alpha(x) = \sum_n a_n e^{i\, n\, f_\alpha(x)}, \tag{5}$$

where $\alpha = p, q$, $f_p(x) = \frac{2\pi}{p_a}log(p_c+p_a x)$, $f_q(x) = q_c x + \frac{1}{2}q_a x^2$, a_n are the Fourier coefficients of the grating, and n are entire numbers.

On the other hand, the field after the q-CG can be described as

$$u_{1,q}(x) = u_0(x)t_q(x) \propto e^{-\frac{(x-x_g)^2}{\omega_0^2}} \sum_n a_n e^{i\, n\, \left(q_c x + \frac{1}{2}q_a x^2\right)}. \tag{6}$$

The far field intensity distribution is obtained using Fraunhofer approximation by solving

$$u_q(\theta) \propto \int_{-\infty}^{+\infty} u_{1,q}(x) e^{-i\,k\,x\,sin\theta} dx, \tag{7}$$

where $k = 2\pi/\lambda$ is the wavenumber. This integral for q-CGs is easily solved, since there are only linear and quadratic terms in the exponential, resulting

$$u_q(\theta) \propto \sum_n \frac{a_n}{\sqrt{2 - in\,q_a\omega_0^2}} e^{-\left(\frac{x_g}{\omega_0}\right)^2} e^{-\frac{\left(k\,sin\theta - n\,q_c + 2ix_g/\omega_0^2\right)^2}{4/\omega_0^2 - 2i\,n\,q_a}}. \tag{8}$$

When there is not interference between orders, the intensity distribution at the far field results in $I_\alpha(\theta) = \sum_n u_n(\theta) u_n^*(\theta)$, being u_n the amplitude for each diffraction order. Considering Eq. (8), we obtain

$$I_q(\theta) \propto \sum_n \frac{|a_n|^2}{\omega_q} e^{-\frac{[k\,sin\theta - n\,(q_c + q_a x_g)]^2}{\omega_{n,q}^2}}, \tag{9}$$

where $\omega_{n,q} = \sqrt{2}\sqrt{(1/\omega_0)^2 + (n\,q_a\,\omega_0/2)^2}$ is the angular width of the diffraction order n. For the limit $q_a \to 0$ we recover the far field diffraction pattern produced by a periodical grating. Now, let us analyze which are the differences between standard periodic gratings and q-CGs. In the first place, we can see that q-CGs produce diffraction orders which propagate following the grating equation, where the frequency for determining the angular separation of orders is that at the center of the Gaussian beam:

$$k\,sin\theta = n\,(q_c + q_a x_g). \tag{10}$$

These diffraction orders present a total power proportional to $|a_n|^2$. On the other hand, the angular width of diffraction orders, $\omega_{n,q}$, is not constant but it increases with the diffraction order n and the chirping parameter q_a. In Fig. 2a we can see an example of far field diffraction pattern obtained with Eq. (9). It is clear that the width of the diffraction orders is not equal, as for the case of constant period diffraction gratings, but depends on the order. This far field diffraction pattern is compared to that obtained numerically with the Fast Fourier Transform of the field after the grating $|FFT[u_{1,q}(x)]|$. There is an excellent agreement between analytical and numerical approaches.

For the case of p-CGs, that is, gratings with a linear variation in the period, the integral required to determine the far field diffraction pattern

$$u_p(\theta) \propto \sum_n a_n \int_{-\infty}^{+\infty} e^{-(x-x_g)^2/\omega_0^2} e^{i\,n\,\frac{2\pi}{p_a} log(p_c + p_a x)} e^{-i\,k\,x\,sin\theta} dx, \tag{11}$$

cannot be solved analytically, and an approximation is required. For this, we have performed a quadratic series expansion of logarithm in second exponential resulting in

$$e^{i\,n\,\frac{2\pi}{p_a} log(p_c + p_a x)} \approx e^{i\frac{2\pi n}{p_a}\left[log(p_c) + \frac{p_a}{p_c}x - \frac{p_a^2}{2p_c^2}x^2\right]}.$$

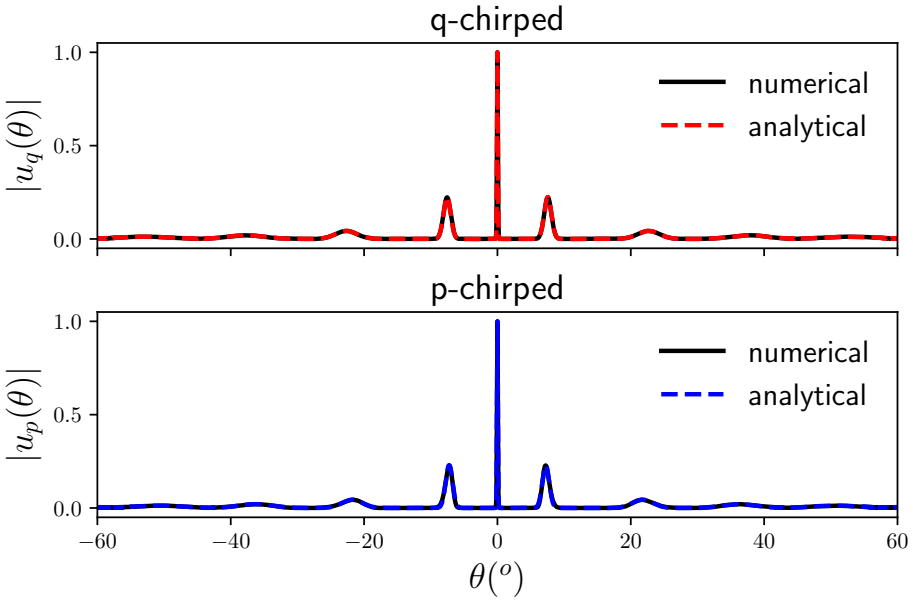

Figure 2: Numerical and analytical diffraction pattern at the far field produced by a q- and a p-CG. The incident beam presents a Gaussian profile with $\omega_0 = 125\,\mu m$, the wavelength is $\lambda = 0.6328\,\mu m$, and impinges in normal incidence to the grating at $x_g = 0\,\mu m$. Both q- and p-CGs present a size $L = 500\,\mu m$, and initial and final periods $p_0 = 6\,\mu m$ and $p_1 = 4\,\mu m$ respectively. Then $q_a = 0.0010\,\mu m^{-2}$ and $p_a = -0.004$.

With this approximation, the intensity results

$$I_p(\theta) \propto \sum_n \frac{|a_n|^2}{\omega_{n,p}} exp^{-\frac{\left[k\,sin\theta - n\frac{2\pi}{p_c}(1-\frac{p_a}{p_c}x_g)\right]^2}{\omega_{n,p}^2}}, \tag{12}$$

where $\omega_{n,p} = \sqrt{2}\sqrt{(1/\omega_0)^2 + (\pi n\, p_a\, \omega_0/p_c^2)^2}$. Obviously, when $p_a = 0$, we recover the far field pattern of a standard diffraction grating. Similarly to the case of q-CG, the width of diffraction orders is not constant but it increases with the order n. In Fig. 2b we can see the diffraction pattern produced by a p-CG with the same parameters as Fig. 2a. As predicted, p-CGs are governed by standard grating equation where the period in the equation is that at the center of the beam

$$\frac{p_c}{(1-\frac{p_a}{p_c}x_g)}\, sin\theta \approx (p_c + p_a x_g)\, sin\theta = n\lambda. \tag{13}$$

The quotient is due to approximation performed to obtain Eq. (12).

In Fig. 2, both p-chirped and q-CGs produces similar diffraction patterns, since the q_a and p_a parameters are small. However, this is not always the case. For example, in Fig. 3, we can see that the diffraction patterns produced by q- and p-chirped gratings are quite different, since q-chirped grating produces wider diffraction orders than p-chirped grating. This can be seen comparing the widths given in Eq. (9) and Eq. (12), $\omega_{n,q}$ and $\omega_{n,p}$, using the definition of parameters, given in Eq. (1).

Finally, we calculate the far field diffraction pattern produced by a CG of finite size illuminated by a plane wave. This case is more realistic in many practical applications. For the case of a q-CG, the integral to solve is

$$u_q|_{p-w}(\theta) \propto \int_{-L/2}^{+L/2} \sum_n a_n e^{i\,n\left(q_c x + \frac{1}{2}q_a x^2\right)} e^{-i\,k\,x\,sin\theta} dx, \tag{14}$$

resulting in

$$\begin{array}{c} u_q|_{p-w}(\theta) \propto a_0 L\, sinc\left(\frac{L}{2}k\, sin\theta\right) \\ + \left(\frac{1+i}{2}\right)\sqrt{\frac{\pi}{q_a}}\sum_{n\neq 0}\frac{a_n}{\sqrt{n}} e^{-i\frac{(n\,q_c - k\,sin\theta)^2}{2nq_a}} \\ \times \left(erf\left[\left(\frac{1-i}{2}\right)\frac{k\,sin\theta - nq_0}{\sqrt{nq_a}}\right] - erf\left[\left(\frac{1-i}{2}\right)\frac{k\,sin\theta - nq_1}{\sqrt{nq_a}}\right]\right), \end{array} \tag{15}$$

where $sinc = sin(x)/x$ and $erf(x) = 2/\sqrt{\pi}\int_0^x exp(-t^2)dt$ is the error function. Since the erf function approximately behaves like a step function, eq. (15) provides a simple relation for the starting and final frequencies of the diffraction orders, which is given when the erf function is null, that is,

$$k\, sin\theta_0 = nq_0 \text{ and } k\, sin\theta_1 = nq_1. \tag{16}$$

As a consequence, we can select the angular width of a diffraction order by the initial and final periods of the grating: $sin\theta_n \in (sin\theta_0, sin\theta_1) = (nq_0/k, nq_1/k)$.

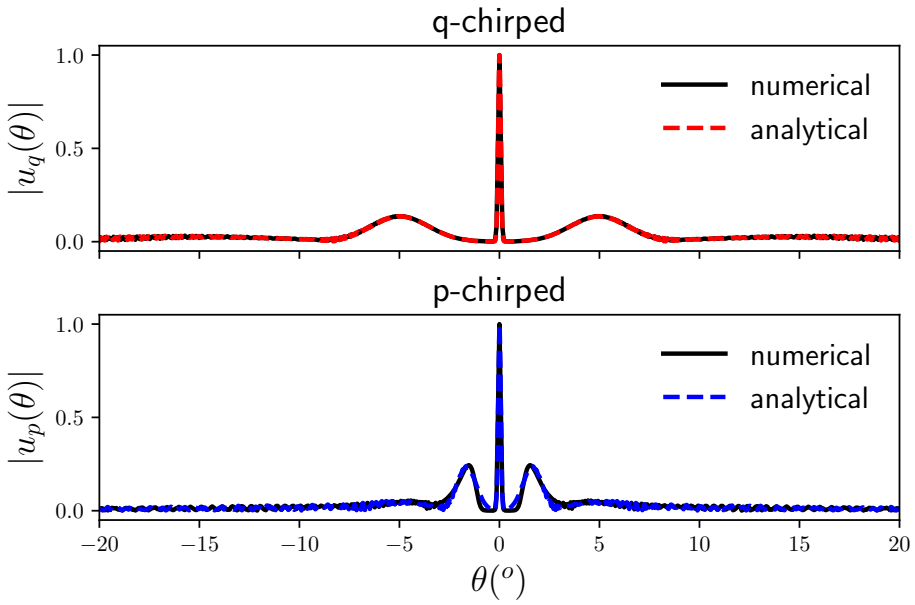

Figure 3: Numerical and analytical diffraction pattern at the far field produced by a q- and a p-CG with the same conditions than in Fig. 2 except initial and final periods which are $p_0 = 40\,\mu m$ and $p_1 = 4\,\mu m$. Then $q_a = 0.0028\,\mu m^{-2}$ and $p_a = -0.072$.

On the other hand, for a p-CG, the integral to solve is

$$u_q|_{p-w}(\theta) \propto \int_{-L/2}^{+L/2} \sum_n a_n e^{i\,n\,\frac{2\pi}{p_a}\log(p_c+p_a x)} e^{-i\,k\,x\,sin\theta} dx, \tag{17}$$

resulting in

$$\begin{aligned} u_q|_{p-w}(\theta) &\propto a_0 L\, sinc\left(\tfrac{L}{2}k\, sin\theta\right) \\ &+ \tfrac{i}{k\sin\theta} e^{i\frac{kp_c\sin\theta}{p_a}} \textstyle\sum_{n\neq 0} a_n \left(\frac{-ik\sin\theta}{p_a}\right)^{\frac{-2in\pi}{p_a}} \\ &\times \left[\Gamma\left(1+\tfrac{2in\pi}{p_a}, i\tfrac{kp_0 sin\theta}{p_a}\right) - \Gamma\left(1+\tfrac{2in\pi}{p_a}, i\tfrac{kp_1 sin\theta}{p_a}\right)\right], \end{aligned} \tag{18}$$

where $\Gamma(a,z) = \int_a^\infty t^{a-1}e^{-t}dt$ is the upper incomplete gamma function.

In Fig. 4 we can see a comparison between analytical and numerical results for a q-CG (parameters given at caption). The total power of the diffraction orders is distributed between angles (θ_0, θ_1) and a constant distribution of the intensity is obtained for q-chirped gratings. Also, the numerical results for a p-CG are presented. Nevertheless, a simple equation for the far field intensity distribution is not possible for comparison. We can see that the intensity distribution in the diffraction orders is not constant for this case.

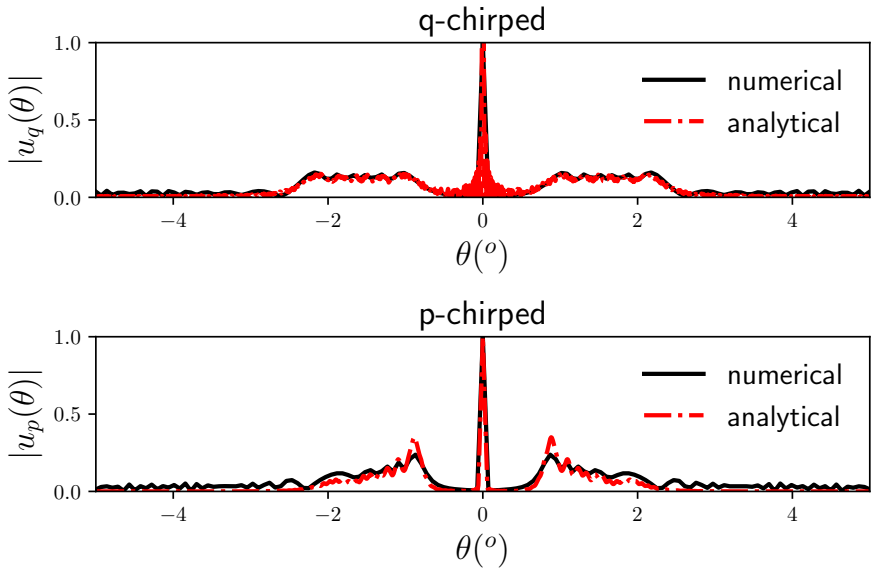

Figure 4: Numerical and analytical diffraction pattern at the far field produced by a q-CG and p-CG illuminated by a plane wave whose wavelength is $\lambda = 0.6328\,\mu m$, and impinges in normal incidence to the grating. The length of the grating is $L = 500\,\mu m$, and initial and final periods $p_0 = 50\,\mu m$ and $p_1 = 15\,\mu m$ respectively. Then $q_a = 0.272\,\mu m^{-2}$ and $p_a = -0.07$.

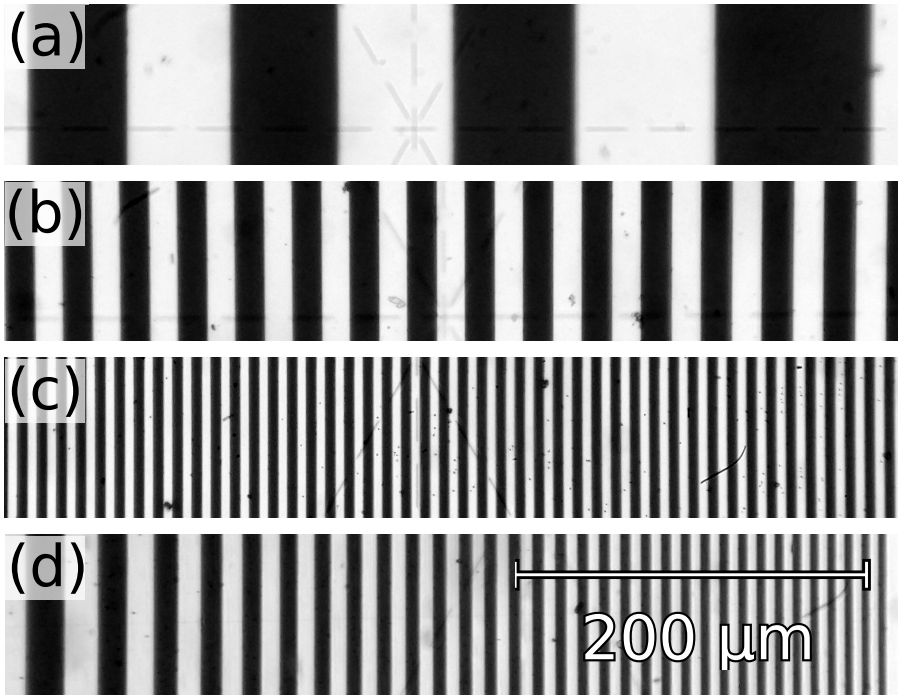

Figure 5: Images of different areas of the q-CG (A) of L = 10 mm fabricated by photolithography with chromium on quartz. (a) Initial period at x=-L/2, (b) at x=0 and (c) at x=L/2. (d) Image of the q-CG (B) of L = 0.5 mm (detailed description in text).

3. Experimental results

To corroborate the analytical formalism we have performed an experimental verification of the far field intensity distribution using two q-CGs fabricated with (A): L = 10 mm, $q_0 = 0.02\mu\text{m}^{-1}$, and $q_1 = 0.299\mu\text{m}^{-1}$ ($p_0 = 314\,\mu$m, $p_1 = 21\mu$m), shown in Fig. 5 (a) to (c), and (B): L = 0.5 mm, $q_0 = 0.0125\mu\text{m}^{-1}$, and $q_1 = 0.640\mu\text{m}^{-1}$ ($p_0 = 50\,\mu$m, $p_1 = 9.81\mu$m), shown in Fig. 5 (d).

The gratings are illuminated by a He-Ne laser beam by Melles Griot of 5 mW power and wavelength $\lambda = 632.8\,nm$. The experiment consists of acquiring the intensity distribution with a UI-1490LE-M-GL IDS camera (1/2 inch sensor) with a pixel lateral size of 1.67 μm and an objective Fujinnon 9 mm/f1.4. We have used the chirped grating (A) to demonstrate the far field using a Gaussian light beam, and chirped grating (B) to demonstrate the far field using a plane-wave. For the latter experiment we have used also a beam-expander to illuminate uniformly the grating and capture the reflected intensity of the projected far-field.

The intensity distribution for a Gaussian beam after illuminating the grating (A) is shown in Fig. 6. We have fitted the experimental intensity with Eq. (9) finding the position of illumination, x_g=4.7mm. In fact, a linear displacement

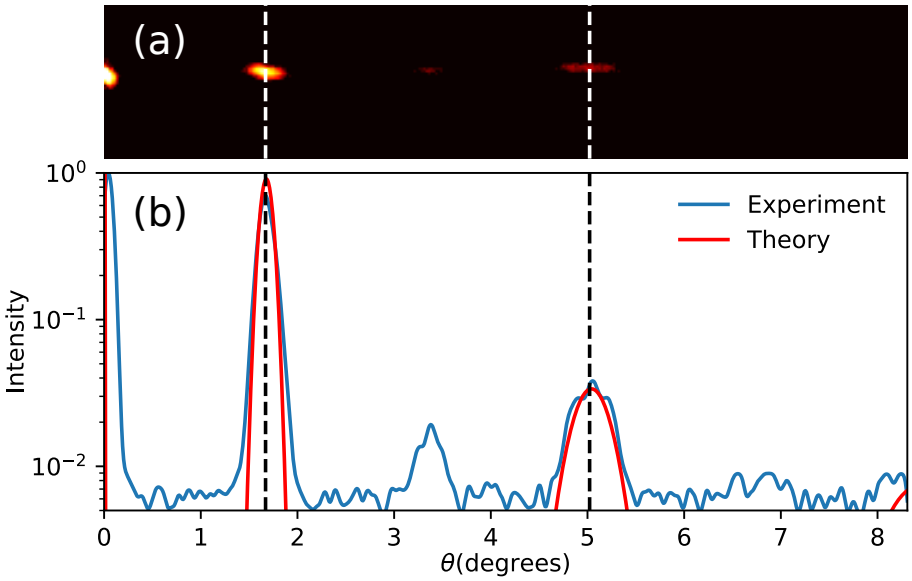

Figure 6: Experimental far-field intensity distribution for CG (A) illuminated with a Gaussian light beam. (a) Intensity obtained from the camera. (b) Intensity distribution of the far field, obtained from the camera sensor (blue-line) and from Eq. (9) (red-line). The vertical dashed lines are the maximum of intensity for the first and third order respectively.

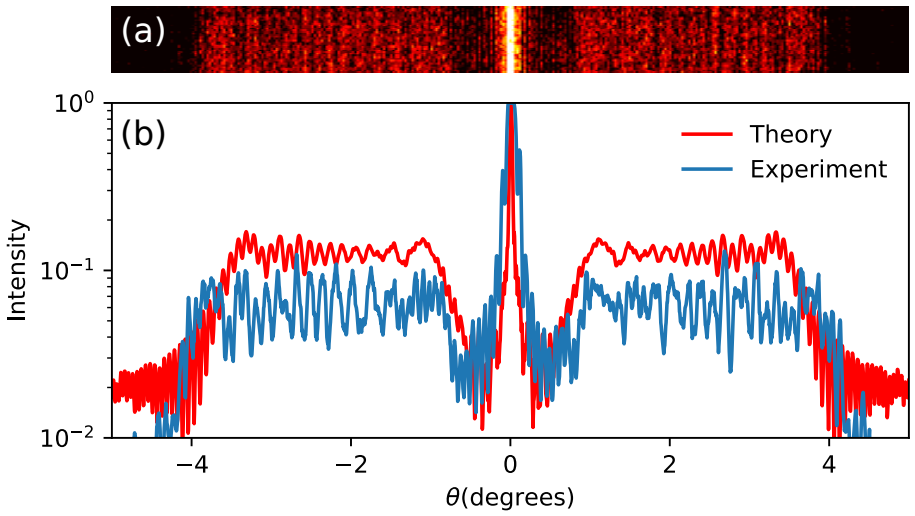

Figure 7: Experimental far-field intensity distribution for CG (B) illuminated with a plane wave. (a) Intensity obtained from the camera. (b) Intensity distribution of the far field, obtained from the camera sensor (blue-line) and from Eq. (15) (red-line).

of the laser source over the diffraction grating will modify the spatial frequency illuminated by the laser beam and, consequently, the angular far-field intensity. Also, it is important to note from Fig. 6 that the second order is not zero because the filling factor of the fabricated grating is not exactly 50/50.

On the other hand, the intensity distribution for an uniform beam after illuminating grating (B) is shown in Fig. 7. For diffraction order $n = 0$, a narrow sinc convoluted signal is obtained. It is more relevant to note that the experimental and analytical curves present a flat widening of the first order, compared to the zero order, which is associated, as shown analytically, to each local spatial frequency found in the q-grating.

4. Discussion

We have seen a different behavior of chirped grating depending on the value of the chirped parameter q_a and the illumination type (Gaussian or plane wave). Now, let us consider two applications that can be developed using spatial CGs. In the first case, let us consider a long chirped grating with a low q_a parameter illuminated with a narrow Gaussian beam. This is the case of q-CG (A) shown in Fig 5(a-c). The scheme of this application can be seen in Fig. 8(a). The light beam sees approximately a constant period grating and diffraction orders are deflected according to standard grating equation, Eq. (10) for q-chirped gratings or Eq (13) for p-chirped gratings. Therefore, a lateral displacement Δx of the grating produces symmetric variation in the deflection angle of diffraction orders, as it is shown in Fig. 8(b).

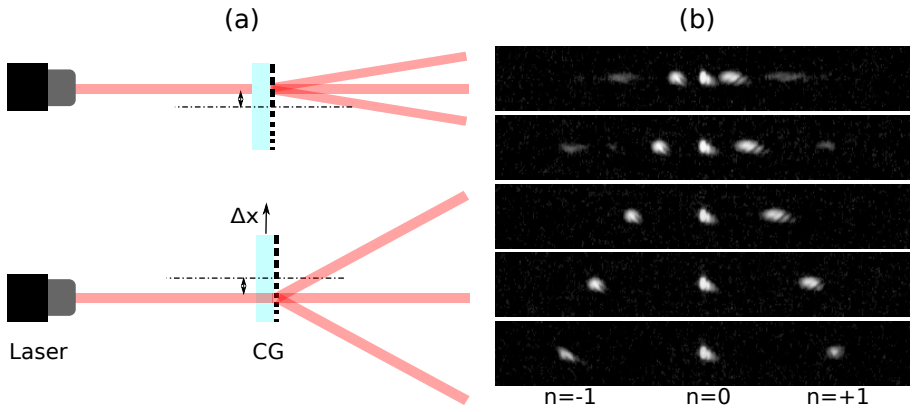

Figure 8: (a) Scheme of how a CG with low q_a parameter can be used as a deflector: depending on the position that the laser beam impinges the grating, the deflection angle with be different. (b) Experimental demonstration of selectable deflection beam. (video showing deflection.)

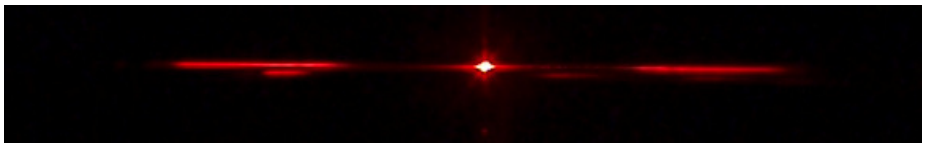

Figure 9: Experimental image of diffraction order widening of high q_a chirped grating, q-CG (B) grating. The small light line below order $n = -1$ is due to a reflection in the objective.

A second application of chirped diffraction gratings can be developed for high q_a parameter CG, such as q-CG (B) grating of Fig. 5. When this grating is illuminated with a plane wave, diffraction orders $|n| \geq 1$ present a high widening, as it is shown in Fig. 9. The width of these orders can be selected with the initial and final periods of the grating: $sin\theta_0 = n\lambda/p_0$ to $sin\theta_1 = n\lambda/p_1$. The intensity distribution of the diffraction order depends on the spatial variation of period, but this intensity distribution is uniform, as it is shown in Fig. 9.

5. Conclusion

In this work we analyze the far-field behavior of chirped diffraction gratings with a linear dependence in the period and in the spatial frequency. Simple analytical expressions for the intensity distribution are obtained which show that, when the chirped grating is illuminated with a Gaussian beam, the width of the diffraction orders depends on the slope of the period, p_a, or the spatial frequency, q_a, respectively. The analytical equations obtained are in good agreement with the numerical simulations and experimental results. These CGs can be used to obtain a simple device for deflecting diffraction orders with a desired tunable angle, which can be of interest in applications such as photonics, metrology,

spectroscopy, etc. Also, CGs can be used for generating diffraction orders with the desired angular width.

Acknowledgments

This work has been funded by project Retos Colaboración 2016 "Ecograb" RTC-2016-5277-5 of the Ministerio de Economía y Competitivdad and the European Union, European funds for regional development.

References

[1] Z. Bomzon, V. Kleiner, E. Hasman, Computer-generated space-variant polarization elements with subwavelength metal stripes, Optics Letters 26 (1) (2001) 33–35.

[2] E. E. Moon, L. Chen, P. N. Everett, M. K. Mondol, H. I. Smith, Nanometer gap measurement and verification via the chirped-Talbot effect, Journal of Vacuum Science & Technology B 22 (6) (2004) 3378–3381.

[3] A. April, N. McCarthy, ABCD-matrix elements for a chirped diffraction grating, Optics Communications 271 (2) (2007) 327 – 331.

[4] S. Kim, Y. Lim, H. Kim, J. Park, B. Lee, Optical beam focusing by a single subwavelength metal slit surrounded by chirped dielectric surface gratings, Applied Physics Letters 92 (1) (2008) 013103.

[5] W.-H. Yeh, J. Kleingartner, A. C. Hillier, Wavelength tunable surface plasmon resonance-enhanced optical transmission through a chirped diffraction grating, Anal. Chem. 82 (12) (2010) 4988–4993.

[6] Q. Gan, F. J. Bartoli, Surface dispersion engineering of planar plasmonic chirped grating for complete visible rainbow trapping, Applied Physics Letters 98 (25) (2011) 251103.

[7] L. M. Sanchez-Brea, F. J. Torcal-Milla, T. Morlanes, Near-field diffraction of chirped gratings, Optics Letters 41 (17) (2016) 4091–4094.

[8] M. C. Hettrick, Divergent groove gratings: wavelength scanning in fixed geometry spectrometers, Optics Express 24 (23) (2016) 26646. doi:10.1364/OE.24.026646.

[9] F. J. Torcal-Milla, L. M. Sanchez-Brea, Diffraction by random ronchi gratings, Applied optics 55 (22) (2016) 5855–5859.

[10] F. J. Torcal-Milla, L. M. Sanchez-Brea, Diffraction by gratings with random fill factor, Applied Optics 56 (18) (2017) 5253–5257.

[11] J. Azaña, M. A. Muriel, Temporal self-imaging effects: theory and application for multiplying pulse repetition rates, IEEE Journal of selected topics in quantum electronics 7 (4) (2001) 728–744.

[12] N. Gao, H. Li, X. Zhu, Y. Hua, C. Xie, Quasi-periodic gratings: diffraction orders accelerate along curves, Optics Letters 38 (15) (2013) 2829–2831.

[13] E. Bailey, R. G. Sabat, Surface plasmon bandwidth increase using chirped-pitch linear diffraction gratings, Optics Express 25 (6) (2017) 6904–6913.

[14] M. C. Hettrick, In-focus monochromator: theory and experiment of a new grazing incidence mounting, Applied Optics 29 (31) (1990) 4531–4535. doi:10.1364/AO.29.004531.

[15] L. Xue, S. Brueck, R. Kaspi, Widely tunable distributed-feedback lasers with chirped gratings, Applied Physics Letters 94 (16) (2009) 161102.

[16] H. G. De Chatellus, E. Lacot, W. Glastre, O. Jacquin, O. Hugon, Theory of Talbot lasers, Phys. Rev. A 88 (3) (2013) 033828.

[17] Y. Kato, Optical encoder, European patent EP3026400A1 (2016).
URL `https://www.google.com/patents/EP3026400A1`